OXFORD

Journal of Geophysics and Engineering

Journal of Geophysics and Engineering (2019) **16**, 85–91 doi:10.1093/jge/gxy007

A simple energy-based strategy for sensor orientation in borehole microseismic monitoring

Soledad Lagos[1,2,*] **and Danilo Velis**[1,2]

[1] Universidad Nacional de La Plata, Facultad de Ciencias Astronómicas y Geofísicas, Paseo del Bosque s/n, La Plata (1900), Argentina
[2] Consejo Nacional de Investigaciones Científicas y Técnicas (CONICET), Argentina

*Corresponding author: Soledad Lagos. E-mail: slagos@fcaglp.unlp.edu.ar

Received 2 August 2018, revised 14 September 2018
Accepted for publication 27 November 2018

Abstract

Accurately determining the orientation of borehole sensors is of paramount importance for microseismic monitoring applications. We calculate the relative bearing angle that allows the orientation of borehole receivers for microseismic monitoring by means of an energy-based strategy that considers the recorded horizontal amplitudes of a perforation shot of known position. This process also allows the appropriate separation of P and S waves, enhancing the accuracy of further processing steps (e.g. time arrival picking). By taking into account the inclination and azimuth of the well, this approach searches for the angle that, after the proper rotations are applied, leads to maximum energy in the source–receiver direction (and minimum energy in the transverse direction). We test the method on synthetic records and two field datasets from Vaca Muerta Formation (Neuquina Basin, Argentina) and statistically evaluate its sensitivity to noise and picking errors. The results show that, in spite of its simplicity, the proposed method is a robust approach that leads to reliable bearing angle estimates with minimum user supervision.

Keywords: Sensor orientation, borehole microseismics, relative bearing angle

1. Introduction

Having precise knowledge of the position and orientation of multicomponent-geophones is essential for borehole microseismic monitoring (Le Calvez *et al.* 2013). Typically, after the sensors are placed within the monitoring well, their positions or 'measured depths' are known. Moreover, the azimuth and inclination of the wells are accurately determined by means of deviation surveys. This information is used to calculate the spatial coordinates of the geophones. Their inclination relative to the vertical direction coincides with the local borehole deviation, but since they rotate as they are deployed, their orientation or relative bearing angle is unknown.

The orientation of sensors is a problem that is not exclusive to microseismic monitoring. For instance, ocean-bottom seismometers also need to be oriented after deployment, a task that can be carried out by considering air-gun recordings or using earthquakes of known position as reference, among other strategies (Anderson *et al.* 1987; Li & Yuan 1999; Stachnik *et al.* 2012). Another typical situation is given by global seismological sensors or magnetotelluric sensors that are oriented relative to the geomagnetic pole in areas where strong geomagnetic anomalies are present (Grigoli *et al.* 2012). Standard techniques employ P-wave polarization analysis to determine the relative orientation between the sensor (or local) coordinate system and the geographic coordinate system (Bulant *et al.* 2007; Huo *et al.* 2016; Greenhalgh & Mason 1995; Li & Yuan 1999) given that in general there are no reference sensors available and absolute values need to be determined. Since the

aforementioned strategies are sensitive to the arrival-time determination and the time-window length considered for the calculations, the accuracy of the results depends significantly on the signal-to-noise ratio. In the case of microseismic monitoring, a few perforation shots are typically considered for the procedure. For the sake of consistency, this process is usually implemented iteratively by updating the individual time picks and window lengths until the orientation angles obtained from different sources reach acceptable deviations, a task that requires an important user interaction. Other strategies use the complete waveforms. Although they are more robust, they rely on a reference sensor of known orientation. Therefore, absolute orientation of sensors is obtained from relative solutions (Grigoli *et al.* 2012; Krieger & Grigoli 2015). If sensor orientations are determined in this way, the error accumulation needs to be assessed. Ekström & Busby (2008) use synthetic seismograms to cross-correlate with the records to obtain the orientation of sensors. Synthetic seismograms are generated from known source parameters of cataloged earthquakes, which are not available in microseismic monitoring scenarios. Zeng & McMechan (2006) combine an analytic solution proposed by DiSiena *et al.* (1984), which is based on power maximization, with a relative-angle cross-correlation-based strategy, and obtain the azimuthal orientation of sensors by a least-squares fitting over a large number of shots (sources of known position).

In this work we show the implementation of an easy yet effective strategy to calculate the relative bearing angles of borehole geophones using an energy-based criterion. Verticality of the monitoring well is not required as long as its deviation and azimuth information was available, as in the case of the slightly deviated wells of the examples considered in this work. We show that changes in the window lengths or errors in the time picks barely influence the results, provided that enough P-wave information is encompassed within the selected window. We consider a synthetic example and two datasets of real microseismic perforation shots to show that, despite its simplicity, this strategy is robust and requires minimal user supervision.

2. Methodology

Figure 1 illustrates the coordinate reference systems associated with a single sensor within a deviated well.The geophone plane and axis correspond to the local system, given by the three components of the geophone. The z-axis of the geophone coincides with the local direction of the well, deviated from the vertical direction v by an angle i. The horizontal plane is defined by the direction x', which is given by the azimuth α of the well (measured clockwise from North), and its perpendicular direction y'. The angle Ω is the *relative bearing angle*, which is measured on the geophone plane between the y and y' directions. The angles i, α and Ω define the rotations that link the geophone and geographic coordinate systems. Thus, following Becquey & Dubesset (1990), the geographic coordinates (x_g, y_g, v) (relative to the geographic East and North and the vertical direction, respectively) of any point in space can be obtained from its coordinates (x, y, z) in the geophone coordinate system by means of

$$\begin{bmatrix} x_g \\ y_g \\ v \end{bmatrix} = \begin{bmatrix} \sin\alpha & -\cos\alpha & 0 \\ \cos\alpha & \sin\alpha & 0 \\ 0 & 0 & 1 \end{bmatrix} \begin{bmatrix} \cos i & 0 & -\sin i \\ 0 & 1 & 0 \\ \sin i & 0 & \cos i \end{bmatrix} \times \begin{bmatrix} \cos\Omega & \sin\Omega & 0 \\ -\sin\Omega & \cos\Omega & 0 \\ 0 & 0 & 1 \end{bmatrix} \begin{bmatrix} x \\ y \\ z \end{bmatrix}. \quad (1)$$

The three rotation matrices of the right-hand side of equation (1) (all of them counter-clockwise) represent, from right to left, rotations around the z, y' and v axes, respectively. They are indicated as '1', '2' and '3' beside dashed arrows in figure 1. Equation (1) would be the general rotation to apply for location purposes, since the positions of the events need to be referred to the geographic reference frame.

Another rotation could be applied to the data to transform it into a *radial–transverse–vertical* system, being *radial* the horizontal direction between the positions of a perforation shot and the receiver (indicated as r in figure 1). The *transverse* direction is perpendicular to the radial direction, also on the horizontal plane. If β is the azimuth (measured clockwise from North) of the source–receiver direction, then:

$$\begin{bmatrix} r \\ t \\ v \end{bmatrix} = \begin{bmatrix} \sin\beta & \cos\beta & 0 \\ -\cos\beta & \sin\beta & 0 \\ 0 & 0 & 1 \end{bmatrix} \begin{bmatrix} x_g \\ y_g \\ v \end{bmatrix}, \quad (2)$$

which corresponds to a clockwise rotation around the v-axis, indicated as '4' in figure 1.

If all the above rotations are properly applied to the records containing the perforation shot arrivals, the radial component should not contain any S-wave energy but only P-wave energy. Being able to separate P- and S-waves by performing this rotation is useful for improving the arrival time picking and therefore providing better input data for velocity model calibration. The angles i, α and β are generally known. Hence, this approach can be used as a strategy to find the relative bearing angle. For each receiver, we consider the described equations and perform an exhaustive search (in the range $(0, 360°)$ with a 0.5° step) of the angle Ω for which the energy in the radial component is maximum and the energy in the transverse component is minimum, within a time window that contains the P-wave. Mathematically, the problem consists of the maximization of the function

$$J(\Omega) = E_r(\Omega) - E_t(\Omega), \quad (3)$$

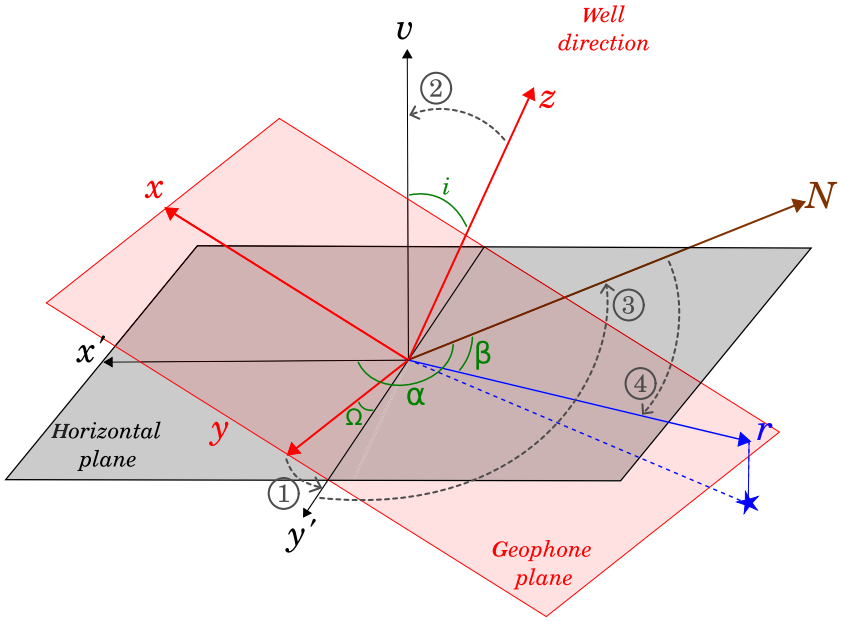

Figure 1. Geophone and geographic coordinate systems and the corresponding rotation angles.

where

$$E_r(\Omega) = \sum_{i=\tau_0}^{\tau_0+N} r_i(\Omega)^2, \quad \text{and} \quad E_t(\Omega) = \sum_{i=\tau_0}^{\tau_0+N} t_i(\Omega)^2 \quad (4)$$

for the radial and transverse components, respectively. The P-wave arrival time, τ_0, in the above equations is manually determined while the length for the time window, N, is chosen beforehand.

There are two possible values for Ω that optimize the objective function of equation (3), which represent a polarity change in the traces. This ambiguity can be assessed by, for example, considering the information in the vertical component of the records, which together with the known position of the source allows the univocal determination of the polarity of each single trace. Another possibility is to compute the sum of all the radial component amplitudes in the time window containing the P-wave, as explained by Zeng & McMechan (2006). If there is certainty that sources are explosions and the polarity is correct, then the amplitude bias should be negative. Therefore, polarity determination could be considered as an additional step in the relative bearing estimation, provided that the time windows containing only the first motion of each trace are carefully selected. We considered including automatic polarity determination for the tests shown in this work. After performing several tests we observed that the above mentioned strategies required a high accuracy in the definition of the first motion time window (arrival times and window length determination). Therefore, in this work we manually chose the polarity after the relative bearing angle estimation. This is possible due to the small number of shots available, which is the general case for microseismic monitoring in hydraulic fracture scenarios.

Due to lateral variations in the velocities, there can be significant differences between actual P-wave polarization and the source–receiver direction (Van Dok *et al.* 2016). However, in such cases the 'radial' direction can be thought of as the direction from which the energy should come from the given source and receiver positions and a 3D velocity model. In other words, if the velocity model presents lateral variation, the radial direction could be determined by means of a 3D ray-tracing instead of the straightforward estimation from the source and receiver positions.

3. Synthetic example

We consider a synthetic example with the aim of evaluating how sensitive to noise this strategy is. For this purpose, we propose a fictitious source modeled as an explosion (diagonal moment tensor) in a homogeneous medium. The corresponding wavefield is registered in an eight-level array deployed within an approximately vertical borehole. Gaussian band-limited noise is added to the records, with different signal-to-noise (S/N) ratios. S/N ratio is calculated as the relation between the maximum absolute amplitude of the signal and the standard deviation, σ, of the noise. We generated 100 records for each S/N ratio from 3 to 5. The proper rotations were applied to account for simulated well azimuth and inclination and sensor relative bearing angles. The simulated relative bearing angles for each geophone are indicated with empty circles in figure 2. The relative bearing angles for each of the 100 realizations for every S/N ratio were

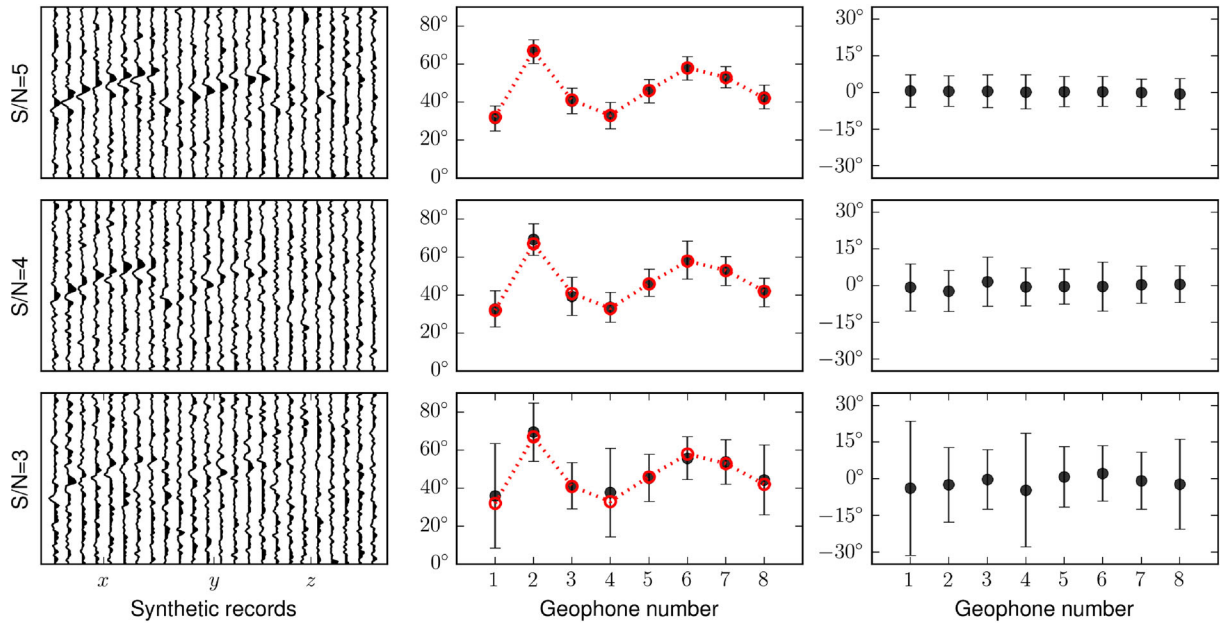

Figure 2. Left: synthetic records for S/N ratios from 3 to 5. Center: actual relative bearing angles (empty circles), and mean estimated relative bearing angles (filled circles) and deviations. Right: corresponding mean errors and deviations.

calculated as described in the previous section. The arrival times and the time window considered is the same for every record. Figure 2 illustrates the results of these tests. The left-hand column in figure 2 shows examples of synthetic records for the different S/N ratios considered. The center column shows the calculated relative bearing angles for each receiver (filled circles) in comparison to the simulated ones (empty circles) and the corresponding standard deviations. The right-hand column shows the corresponding mean errors and standard deviations. As expected, deviations increase with decreasing S/N ratio. However, they only become significant for noise levels that are not typical of perforation shots, which in general are strong events in comparison to ambient noise in borehole microseismic monitoring scenarios. Tests for higher S/N were also performed although not shown in the figure, since deviations for these cases became negligible.

4. Field data example

We tested the method using two datasets of perforation shots carried out in two hydraulic stimulation procedures with the same target formation: Vaca Muerta in the Neuquen Basin, Argentina. 'Dataset 1' is composed of three perforation shots for each of seven stages (21 in total) registered in a seven-level array that was deployed in a nearly-vertical well. For 'dataset 2', only three perforation shots are available. The records correspond to a 10-geophone array, also in a nearly-vertical well. This dataset has a higher S/N ratio than the first one. In both cases, well azimuth and deviation information was available, and velocity models assume no lateral variations.

Figure 3 shows the relative bearing angles obtained for 'dataset 1'. The results for each of the 21 perforation shots are indicated with circles, while the triangles show the corresponding mean values. For figure 3a the raw data was used, while for figure 3b a bandpass filter (30–300 Hz) was previously applied to the perforation shot records. This frequency range was chosen after observing that most of the signal energy was concentrated in that range. Figures 3c and d show the differences between the individual angles and the corresponding means. Figure 4 shows the results corresponding to 'dataset 2', where no filtering was applied nor needed given the high S/N ratio of the data. The arrival times were manually picked, and a fixed length of 20 ms was considered for all time windows. The ambiguity in the traces' polarity was solved manually in order to dispense with a high accuracy in the determination of arrival times and lengths of time windows considered, as explained before.

The results indicate the high consistency attained irrespectively of the perforation shot. In the case of the unfiltered data from 'dataset 1' (figure 3a), although the noise present in the data introduces some dispersion to the solutions, the bandpass filtering allowed us to improve significantly the consistency of the results without introducing errors in the mean values, as shown in figure 5. The differences between the individual and mean relative bearing angles remain smaller than 8° for filtered 'dataset 1' and smaller than 0.5° for 'dataset 2'.

To assess the robustness of the proposed strategy, we performed the following additional tests considering the different conditions that would alter the results.

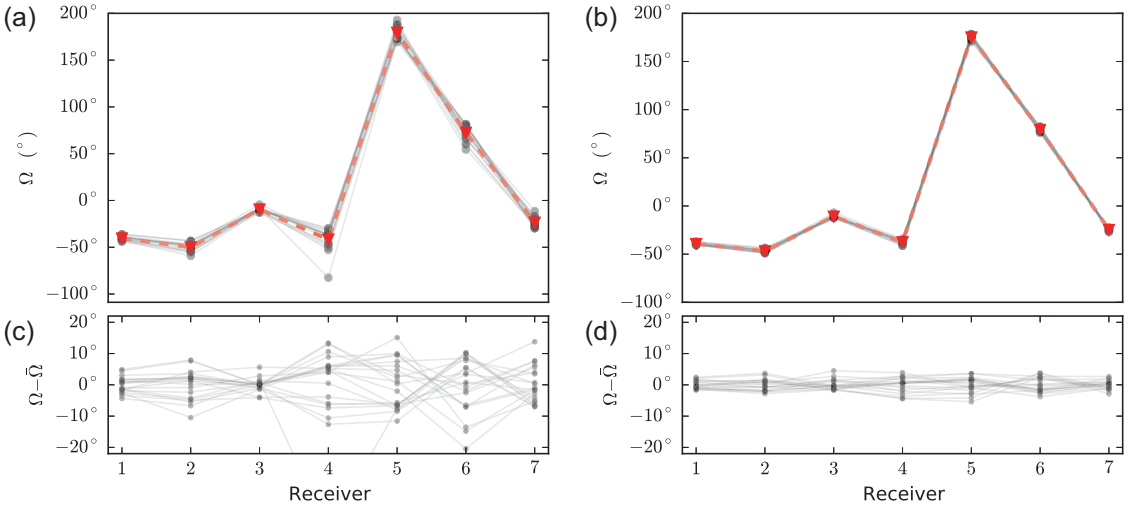

Figure 3. Relative bearing angles calculated for each receiver from individual shots (circles) of 'dataset 1' and mean values (triangles) for (a) raw data and (b) filtered data. (c), (d): results from individual shots minus mean value for cases (a) and (b).

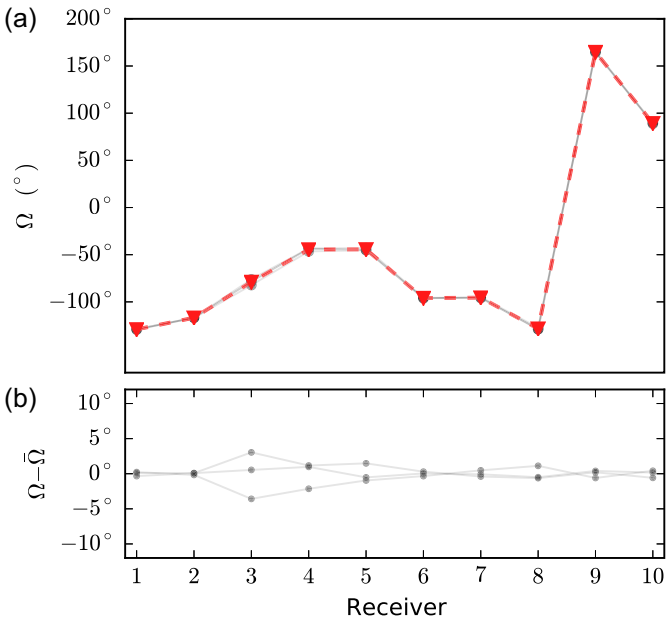

Figure 4. (a) Relative bearing angles calculated for each receiver from individual shots (circles) of "dataset 2" and mean values (triangles). (b) Results from individual shots minus mean value.

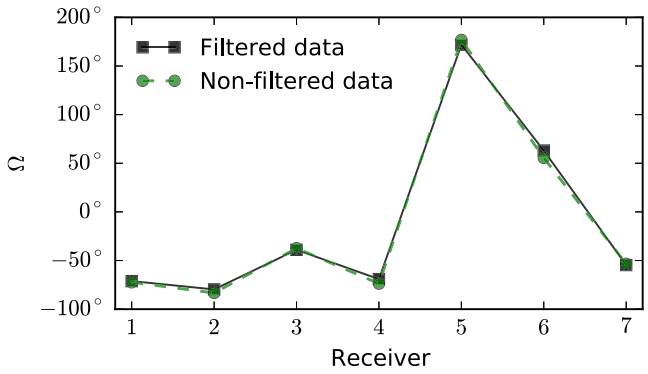

Figure 5. Mean relative bearing angles for raw and filtered data from "dataset 1".

Table 1. Mean relative bearing angles for each receiver, standard deviations and maximum and minimum values obtained after 1000 realizations.

Receiver	Mean	Std	Min	Max
1	−71.1°	1.2°	−73.5°	−68.3°
2	−79.8°	1.8°	−83.3°	−74.0°
3	−38.7°	1.8°	−42.8°	−33.0°
4	−68.6°	2.7°	−74.5°	−60.8°
5	172.2°	2.8°	163.2°	176.0°
6	63.3°	2.4°	59.0°	68.2°
7	−54.6°	1.3°	−58.3°	−51.3°

- Gaussian picking errors with a deviation of $\sigma = 2$ ms. These errors double the expected deviations for microseismic events time-arrival picking (Eisner *et al.* 2010).
- Systematic time arrival biases drawn from a uniform distribution in $[-3, 3]$ ms. Often, these errors are unintentionally introduced either by the analyst during the manual picking process, or by any automatic algorithm that does not accurately determine first breaks but zero-crossings or maximum amplitudes.
- Time-window lengths in the range of from 5 to 40 ms. These variations are intended to simulate the changes that a polarization-based strategy would need. Note that shorter windows may not contain P-wave information at all, while longer windows may contain other phases as well.

We carried out 1000 independent realizations taking into account the above items for each of the 21 shots of 'dataset 1' (a total of 21 000 realizations). Table 1 summarizes the results.

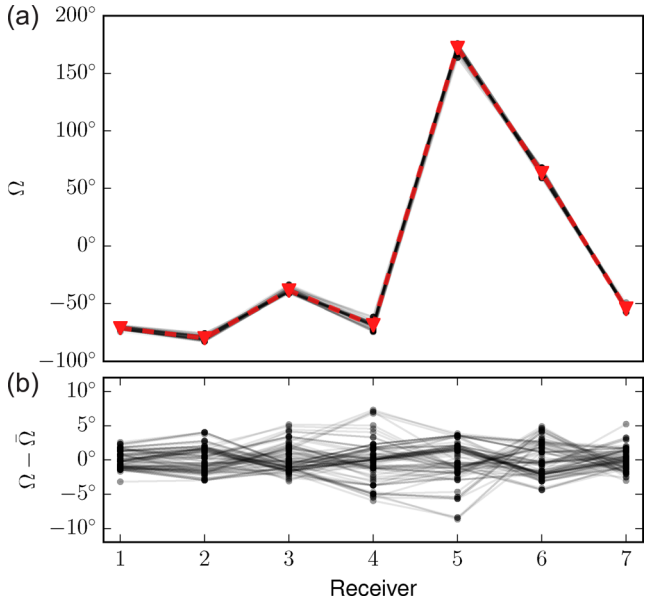

Figure 6. Results of the 1000 realizations (only one in every 200 realizations are illustrated). (a) Relative bearing angles calculated for each receiver from individual shots (circles) of 'dataset 1' and mean values (triangles). (b) Results from individual shots minus mean value.

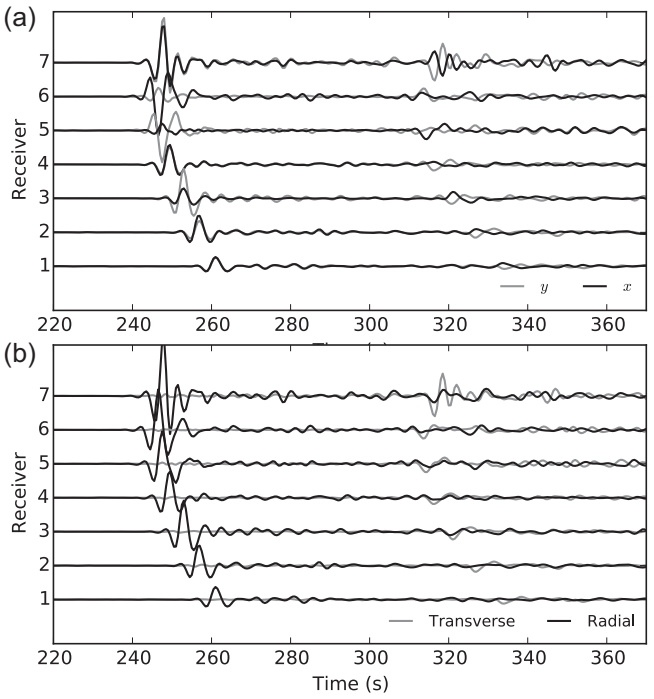

Figure 7. (a) Original record corresponding to a single perforation shot from 'dataset 1'. (b) Record after rotation to the radial–transverse–vertical system using the proposed technique.

The most noteworthy results in this regard are the small deviations obtained despite the different sources of error considered, which include large picking errors and a wide variety of window lengths. Figure 6 depicts one in every 200 realizations. Provided that the P-wave (at least part of it) is contained within the considered time window and that this window does not contain any other phase, the energy-based strategy leads to stable results.

For illustrative purposes, figure 7 shows the record of a single perforation shot before and after rotating to the radial–transverse–vertical system. Observe that the energy of P- and S-waves that was originally mixed in the horizontal components is now clearly separated into two different components.

5. Conclusions

The energy-based strategy implemented as a simple sum of squared amplitudes within a time window containing the P-wave proved to be an easy and effective way of estimating the relative bearing angles. The strategy was tested with synthetic data and two different sets of field data showing satisfactory results in all cases. A large number of tests were performed in order to statistically analyze the results of the relative bearing determinations. These experiments consisted in adding errors to the picked arrival times and modifying the lengths of the time windows. In all cases, standard deviations were small even in defying situations of small time windows or poor arrival-time picking, proving the robustness of this approach. Hence, any automatic arrival-time picker and a fixed window length would be enough for a proper estimation of the relative bearing angles, limiting the user supervision to the polarity correction, if needed.

Acknowledgements

This work was partially supported by Programa de Incentivos, Universidad Nacional de La Plata (UNLP) and Consejo Nacional de Investigaciones Científicas y Técnicas (PIP 112.201201-00626-CO, CONICET), Argentina. The authors would like to thank YPF-Tecnología for supplying the field data used in this work and Germán Brunini for his enriching contributions.

Conflict of interest statement. None declared.

References

Anderson, P., Duennebier, F. & Cessaro, R., 1987. Ocean borehole horizontal seismic sensor orientation determined from explosive charges, *Journal of Geophysical Research*, **92**, 3573–3579.

Becquey, M. & Dubesset, M., 1990. Three-component sonde orientation in a deviated well, *Geophysics*, **55**, 1386–1388.

Bulant, P., Eisner, L., Pšenčík, I. & Le Calvez, J., 2007. Importance of borehole deviation surveys for monitoring of hydraulic fracturing treatments, *Geophysical Prospecting*, **55**, 891–899.

DiSiena, J.P., Gaiser, J.E. & Corrigan, D., 1984. Horizontal components and shear wave analysis of three-component VSP data, in *Vertical Seismic Profiling, Part B: Advanced concepts*, pp. 177–235, ed. Toksöz, M.N. & Stewart, R.R., Geophysical Press.

Eisner, L., Hulsey, B.J., Duncan, P., Jurick, D., Werner, H. & Keller, W., 2010. Comparison of surface and borehole locations of induced seismicity, *Geophysical Prospecting*, **58**, 809–820.

Ekström, G. & Busby, R.W., 2008. Measurements of seismometers orientation at usarray transportable array and backbone stations, *Seismological Research Letters*, **79**, 554–561.

Greenhalgh, S.A. & Mason, I.M., 1995. Orientation of a downhole triaxial geophone, *Geophysics*, **60**, 1234–1237.

Grigoli, F., Cesca, S., Dahm, T. & Krieger, L., 2012. A complex linear least-squares method to derive relative and absolute orientations of seismic sensors, *Geophysical Journal International*, **188**, 1243–1254.

Huo, Y., Zhang, W. & Zhang, J., 2016. Improve sensor orientation using both drop-ball and microseismic events, in *SEG Technical Program Expanded Abstracts, Dallas, Texas, 2016*, Society of Exploration Geophysicists, Tulsa, OK, USA, pp. 2642–2646.

Krieger, L. & Grigoli, F., 2015. Optimal reorientation of geophysical sensors: a quaternion-based analytical solution, *Geophysics*, **80**, F19–F30.

Le Calvez, J., Williams, M. & Couch, J., 2013. Tool and velocity model calibration for downhole-based hydraulic fracture monitoring of induced microseismicity, in *SEG Technical Program Expanded Abstracts, Houston, TX, 2013*, Society of Exploration Geophysicists, Tulsa, OK, USA, pp. 2193–2195.

Li, X. & Yuan, J., 1999. Geophone orientation and coupling in three-component sea-floor data: a case study, *Geophysical Prospecting*, **47**, 995–1013.

Stachnik, J., Sheehan, A., Zietlow, D., Yang, Z., Collins, J. & Ferris, A., 2012. Determination of New Zealand ocean bottom seismometer orientation via Rayleigh-wave polarization, *Seismological Research Letters*, **83**, 704–713.

Van Dok, R.R., Tamimi, N., Fuller, B.N. & Mahrer, K.D., 2016. Do you truly know your geophone's orientation and should you care, in *SEG Technical Program Expanded Abstracts, Dallas, TX, 2016*, Society of Exploration Geophysicists, Tulsa, OK, USA, pp. 2647–2651.

Zeng, X. & McMechan, G.A., 2006. Two methods for determining geophone orientations from VSP data, *Geophysics*, **71**, V87–V97.